

Detached Shell Carbon Stars: Tracing Thermal Pulses on the Asymptotic Giant Branch

JOEL H. KASTNER^{1,2,3} AND EMILY WILSON^{2,4}

¹*Center for Imaging Science, Rochester Institute of Technology, Rochester NY 14623, USA; jhk@cis.rit.edu*

²*School of Physics and Astronomy, Rochester Institute of Technology*

³*Laboratory for Multiwavelength Astrophysics, Rochester Institute of Technology*

⁴*Center for Computational Relativity and Gravitation, Rochester Institute of Technology*

ABSTRACT

We consider whether the subset of carbon-rich asymptotic giant branch (AGB) stars that exhibit detached, expanding circumstellar shells may reveal the past histories of these stars as having undergone helium shell flashes (thermal pulses) on the AGB. We exploit newly available Gaia parallaxes and photometry, along with archival infrared photometry, to obtain refined estimates of the luminosities of all (12) known detached shell carbon stars. We examine the relationship between these luminosities and the estimated dynamical ages (ejection times) of the detached shells associated with the 12 stars, which range from ~ 1000 to ~ 30000 yr. When arranged according to detached shell dynamical age, the (implied) luminosity evolution of the known detached shell carbon stars closely follows the predicted “light curves” of individual thermal pulses obtained from models of AGB stars. The comparison between data and models suggests that detached shell carbon stars are descended from ~ 2.5 – $4.0 M_{\odot}$ progenitors. We conclude that detached shell carbon stars may serve as effective tracers of the luminosity evolution of AGB thermal pulses.

Keywords: Carbon stars (199); Stellar mass loss (1613); Late stellar evolution (911)

1. INTRODUCTION

Intermediate-mass stars that undergo He shell burning on the asymptotic giant branch (AGB) may ultimately be responsible for the generation of most of the free carbon in the Universe (see, e.g., Marigo et al. 2020, and references therein). If sufficient carbon is generated via nucleosynthesis in the deep AGB interior and mixed to the AGB stellar surface, carbon can become more abundant than oxygen by number, resulting in carbon star formation. The study of such carbon-rich AGB stars (hereafter C stars) is essential to trace the enrichment of the ISM in C, as well as in s-process elements that are generated via He shell burning (Herwig 2005).

At solar metallicity, the onset of $C/O > 1$ at an AGB star’s surface likely only occurs very late in AGB evolution, as a direct result of He shell flashes (thermal pulses; hereafter TPs) combined

with repeated “third dredge-up” episodes, i.e., periods of internal convection and mixing that are sufficiently robust so as to bring the products of He shell burning to the surface (Herwig 2005). Furthermore, inversion of the C/O ratio is only theoretically predicted to occur for a relatively narrow range of main-sequence progenitor masses, with the range being highly dependent on initial metallicity and the (poorly constrained) details of stellar mixing and convection (e.g., Marigo et al. 2008). In the Galaxy, there is observational evidence that only stars of initial mass $\geq 1.65 M_{\odot}$ will evolve to become C stars (Marigo et al. 2020). The upper end of the C star progenitor mass range, which is more difficult to constrain observationally (e.g., Kastner et al. 1993), is predicted to lie at $\sim 4.5 M_{\odot}$ for solar metallicity (Karakas 2014).

The C-rich dust generated in cool, highly extended C star photospheres has large opacity to optical/IR photons, making radiation pressure on dust a particularly efficient mass loss mechanism for such stars (Höfner & Olofsson 2018). As a consequence, most C stars exhibit large mass loss rates ($\sim 10^{-7}$ – $10^{-5} M_{\odot} \text{ yr}^{-1}$; Olofsson et al. 1993; Höfner & Olofsson 2018, and references therein). Their expanding circumstellar molecular envelopes, readily detectable in millimeter-wave CO emission lines and the thermal infrared spectral signatures of C-rich dust, are characterized by large inferred CO:H₂ ratios and an array of trace C-bearing molecules (Höfner & Olofsson 2018).

A subset of C stars also display extended, thin shells of ejecta that are detached from the stars. The first handful of such “detached shell C stars” were detected via analysis of their CO line profiles (Olofsson et al. 1988, 1990, 1992), with most of these detached shells later confirmed via single-dish and/or interferometric mapping (e.g., Olofsson et al. 1996; Maercker et al. 2016; Kerschbaum et al. 2017). Another handful, some with no known molecular gas (CO) counterparts, were detected via thermal IR imaging (Izumiura et al. 1996; Kerschbaum et al. 2010; Mečina et al. 2014). More recently, a detached shell associated with the C star TX Psc was identified via interferometric CO mapping (Brunner et al. 2019).

At the time of the discovery of the first such systems, it was hypothesized that each detached shell now coasting away from a C star is likely the direct result of the impulsive luminosity increase during a TP (Olofsson et al. 1990, 1992). Theoretical support for such a direct, causal connection has since steadily accumulated (e.g., Steffen et al. 1998; Mattsson et al. 2007; Maercker et al. 2012). In this paper, we explore one potential observational manifestation of the potential connection between C star TPs and detached shells: the relationship between the present-day luminosities of the dozen known detached shell C stars and the dynamical ages of their ejected shells. We exploit newly available Gaia parallaxes and photometry, along with archival infrared photometry, to calculate the luminosities of all (12) known detached shell carbon stars, and to obtain refined estimates of their shell ejection timescales. We place these results in the context of models of thermally pulsing AGB stars to assess whether detached shell carbon stars might trace the luminosity evolution of AGB thermal pulses.

2. SAMPLE AND DATA

The list of known detached shell C stars, compiled from Olofsson et al. (1988, 1990, 1992, 1996), Izumiura et al. (1996), Izumiura et al. (2011), Lindqvist et al. (1999), Schöier et al. (2005), Kerschbaum et al. (2010), Mečina et al. (2014), and Brunner et al. (2019), is presented in Table 1. The Table lists parallaxes (π) for these stars as obtained from the Hipparcos and Gaia EDR3 catalogues (van Leeuwen 2007; Gaia Collaboration et al. 2021). The Gaia EDR3 parallax uncertainties include the estimated systematic astrometric error (`astrometric_excess_error`), added in quadrature to

Table 1. DETACHED SHELL CARBON STARS: PARALLAXES AND DISTANCES

Object	Hipparcos π (mas)	Gaia EDR3 π (mas)	RUWE	$1/\pi$ ($\sigma_{1/\pi}$) (pc)	Src. ^a	D (BJ21 ^b) (pc)
U Cam	0.79±1.35	1.62±0.29	0.95	618 (109)	G	604 ⁺¹² ₋₁₃
DR Ser	0.59±1.48	0.91±0.22	1.00	1103 (267)	G	1054 ⁺³¹ ₋₃₂
V644 Sco	...	0.74±0.17	0.74	1353 (306)	G	1279 ⁺⁵⁰ ₋₄₃
R Scl	2.11±1.75	2.54±0.56	2.55	394 (80)	G	388 ⁺¹² ₋₁₀
TX Psc	4.29±0.93	4.09±1.09	1.92	233 (51)	H	243 ⁺¹² ₋₁₁
U Ant	3.9±0.67	3.62±0.79	1.03	256 (44)	H	276 ⁺⁶ ₋₇
TT Cyg	1.96±0.8	1.44±0.16	1.03	695 (75)	G	618 ⁺⁸ ₋₁₀
S Sct	2.53±0.9	2.36±0.29	0.82	424 (53)	G	415 ⁺¹⁰ ₋₈
U Hya	6.18±0.75	162 (20)	H	...
AQ And	...	1.26±0.15	1.00	794 (96)	G	769 ⁺¹⁶ ₋₁₈
RT Cap	1.78±1.48	1.80±0.24	0.82	556 (74)	G	542 ⁺¹⁴ ₋₁₃
Y CVn	4.59±0.73	3.22±1.30	1.97	218 (35)	H	314 ⁺¹⁷ ₋₁₈

NOTES: a) Source for distance in column 5: G = straight inverse of Gaia EDR3 parallax; H = straight inverse of Hipparcos parallax. b) Gaia EDR3 distance from [Bailer-Jones et al. \(2021\)](#).

Table 2. DETACHED SHELL CARBON STARS: PHOTOMETRY^a

Band ^b λ (μm)	B_P	V	G	R_P	J	H	K_s	W1	W2	S9W	W3	12	L18W	W4	25	60	100	N160	$E(B-V)$
	0.50	0.55	0.58	0.76	1.24	1.65	2.17	3.35	4.60	8.62	11.57	11.60	18.4	22.1	23.9	61.9	102	160	
U Cam	3.14	3.51	16.4	41.1	187	395	422			133		121	39.3		40.9	16.9	7.31		0.13
DR Ser	0.423	0.65	2.58	6.69	46.2	106	124	47.5	25.7	21	11	15.9	6.16	5.56	6.66	5.96			0.58
V644 Sco	0.386	0.28	2.44	6.29	38.3	88.1	105	39.2	35	22.7	10.8	17.6		8.26	8.99				0.26
R Scl	9.03	8.57	38.2	92.2	256	554	752			194		162	65.3		82.1	54.8	23.2	5.59	0.01
TX Psc	25.5	35.1	92.1	192	524	1060	1080			174	95.7	150	45.4	32.6	41.9	13.4	7.27		0.08
U Ant	16.7	23	68.2	158	591	1190	1270	717 ^c	224 ^c	264	111	168	61.5	35.8	44.8	27.1	21.1		0.04
TT Cyg	2.69	3.23	9.19	20.6	52.1	102	111		37.6	20.4	8.08	15.8	5.37	3.37	4.17	3.45	4.41		0.09
S Sct	5.18	6.81	21.5	50.7	189	368	379			78.7	50.2	65.3	20.1	13.2	17.3	9.28			0.10
U Hya	27.8	40.3	92.5	194	753	1330	1310			257	87.1	206	78.1	56.5	72.4	17.2	14.5	0.766	0.00
AQ And	1.75	3.11	7.42	17.2	54.1	119	143			32	19.7	25.7	8.16	6.38	7.41	3.83	4.4		0.07
RT Cap	4.09	5.93	18.2	44.6	231	449	510			86.6	43.5	72.9	21.7	15.9	20.7	4.41	3.61	3.79	0.13
Y CVn	23.1	30	84.3	181	634	1360	1330			304	193	276	91.7	57	70.3	17.2	7.82		0.03

NOTES: a) Fluxes in Jy. b) B_PGR_p from Gaia EDR3; JHK_s from 2MASS; W1–4 from WISE; 12, 25, 60, 100 from IRAS; S9W, L18W, N160 from AKARI. c) 3.52 μm and 4.89 μm fluxes from DIRBE.

the formal parallax error. This is appropriate because the systematic error is likely to be statistically significant (i.e., `astrometric_excess_noise_sig` > 3) for all of these stars (see discussion in [Lindgren et al. 2021](#), their § 5.3).

The general utility of Gaia parallax measurements for AGB stars, at least for the more nearby examples, is questionable, due to their large fluxes in the red combined with the fact that their spatially variable photospheres can be resolved by Gaia ([Van Langevelde et al. 2018](#); [Vlemmings et al. 2019](#); [Ramstedt et al. 2020](#)). However, Table 1 demonstrates that the Gaia EDR3 and Hipparcos parallaxes are in agreement, to within the errors, for all stars for which both data sources are available — including the four stars for which both astrometry missions yield parallax measurements with signal/noise ratio >2.5 (TX Psc, U Ant, S Sct, Y CVn), as well as several stars for which the Hipparcos measurements are of lower significance (R Scl, TT Cyg, RT Cap). This comparison

between Gaia EDR3 and Hipparcos parallaxes in Table 1 indicates that the former are, overall, viable measurements for these stars, notwithstanding the fact that three stars have renormalized unit weight error (RUWE) values > 1 (see Table 1), which is a potential indicator of a poor astrometric fit (Lindgren et al. 2021). Indeed, we note that the Gaia EDR3 parallax measured for R Scl — the sample star with the largest RUWE — is in excellent agreement with the distance independently obtained from analysis of light echoes (361 ± 44 pc; Maercker et al. 2018).

We have thus employed Gaia EDR3-based distances for the analysis described in this paper. Specifically, we have adopted the Gaia EDR3-based distances to these stars obtained by Bailer-Jones et al. (2021) from their Bayesian statistical approach, which also accounts for the parallax zero-point offset (although this correction is likely to be negligibly small for the sample stars; Lindgren et al. 2021). In Table 1, we list these distances (D), alongside the distance to each star (and associated distance uncertainty) obtained as the straight inverse of the Gaia or Hipparcos parallax, where we only list the inverse parallax with the greater significance. It is evident that the two distance estimates are in good agreement, with the Bailer-Jones et al. (2021) distances systematically smaller and more (formally) precise than the straight inverse of the Gaia parallaxes, as expected (see discussion in Bailer-Jones 2015). The sole exception is Y CVn, for which the inverse of the Hipparcos parallax is significantly smaller than the Bailer-Jones et al. (2021) Gaia distance. This case is discussed further in § 3.

Photometric data from the Gaia EDR3, 2MASS, WISE, AKARI, and/or IRAS archives, obtained via the Vizier photometry tool¹, are listed in Table 2. These data were used to compile spectral energy distributions (SEDs; Fig. 1) for purposes of determining bolometric fluxes en route to calculating bolometric luminosities (§ 3). The Gaia EDR3 (B_PGR_P) and 2MASS (JHK_s) photometric data were dereddened to account for the estimated line-of-sight interstellar extinction toward each star ($E(B - V)$), listed in Table 2, last column) as obtained from the Bayestar19 (Green et al. 2019) or Stilism (Lallement et al. 2019) Galactic dust extinction maps². For stars with reddening measurements available in both maps (e.g., DR Ser), we report the Bayestar19 value of $E(B - V)$; however, we note that the two maps yield consistent $E(B - V)$ estimates (in the case of DR Ser, which suffers the largest reddening, the Stilism-based estimate of $E(B - V) = 0.56$ is in excellent agreement with the Bayestar19-derived value listed in Table 2). Photometric corrections based on $E(B - V)$ were then applied according to the relations in Schlafly & Finkbeiner (2011).

3. DETACHED SHELL C STARS: LUMINOSITIES AND SHELL AGES

To obtain luminosities for the detached shell C stars, we have calculated their bolometric fluxes (F_{bol}) from the data listed in Table 2. To obtain F_{bol} for each star, we fit a composite of two blackbodies to its dereddened SED, as an approximation of the combination of stellar photosphere plus a contribution from cool circumstellar dust; the photospheric blackbody was normalized to each star’s H band flux. The blackbody fits (Fig. 1) demonstrate that, in all cases, the stellar photospheric emission dominates the bolometric flux (consistent with the results of Schöier et al. 2005). The best-fit blackbody-equivalent effective temperatures (T_{eff}) we find for the detached shell C stars (2300–2800 K; Fig. 1) are generally consistent with previous blackbody-fit-based estimates for many of these same stars (e.g., Schöier & Olofsson 2001; Maercker et al. 2018). These temperatures are systematically

¹ <http://vizier.u-strasbg.fr/vizier/sed/doc/>

² Bayestar19: <http://argonaut.skymaps.info/>; Stilism: <https://stilism.obspm.fr/>

Table 3. DETACHED SHELL CARBON STARS: LUMINOSITIES AND SHELL PARAMETERS

Object	D^a (pc)	L_{bol}^b (L_{\odot})	L_{bol} (Ref.) ^c (L_{\odot})	θ_s ($''$)	v_s (km s ⁻¹)	Refs. ^d	R_s (10 ⁴ au)	τ_s (yr)
U Cam	604	11800	13900 (1)	7.3	23	1	0.44	930
DR Ser	1054	12400	7700 (1)	7.6	20	2, 3	0.80	1940
V644 Sco	1279	11300	15000 (1)	9.4	23.2	4, 5	1.2	2530
R Scl	388	6750	7700 (1)	19.5	14.3	6	0.76	2560
TX Psc	243	5300	6000 (2)	22	10	7	0.54	2590
U Ant	276	7100	6060 (1)	42.5	19	8	1.2	3000
TT Cyg	618	3350	3300 (1)	35	13.3	5	2.2	8100
S Sct	415	5200	5300 (1)	70	17.3	5	2.9	8300
U Hya	162	2800	2960 (3)	110	7.6 ^e	9	1.8	12000
AQ And	769	6150	10400 (4)	55	10 ^f	10	4.2	21000
RT Cap	542	10900	8500 (5)	94	8 ^e	11, 12	5.1	31000
Y CVn	314	10600	9100 (5)	190	8 ^e	13, 12	6.0	36000

NOTES:

a) From Table 1.

b) L_{bol} obtained from our blackbody fitting (see §3). c) Literature L_{bol} value (with reference in parentheses), corrected for the distance listed in column 2.

References: 1. Schöier et al. (2005); 2. Brunner et al. (2019); 3. Izumiura et al. (2011); 4. Kerschbaum et al. (2010); 5. Schöier & Olofsson (2001).

d) References for detached shell angular diameters (θ_s) and expansion velocities (v_s): 1. Lindqvist et al. (1999); 2. Ramstedt et al. (2011); 3. Schöier et al. (2005); 4. Maercker et al. (2018); 5. Olofsson et al. (1996); 6. Maercker et al. (2016); 7. Brunner et al. (2019); 8. Kerschbaum et al. (2017); 9. Izumiura et al. (2011); 10. Kerschbaum et al. (2010); 11. Mečina et al. (2014). 12. Olofsson et al. (1993); 13. Izumiura et al. (1996).

e) Expansion velocity obtained from spatially integrated CO line profile; possibly dominated by present-day mass loss.

f) Assumed shell expansion velocity.

lower than the T_{eff} values obtained by Bergeat et al. (2001) via modeling of C star atmospheric spectral features, for the stars in common. However, we find that the Wien tails of blackbodies fixed to the Bergeat et al. (2001) T_{eff} values overshoot the stars' optical fluxes, with the result that F_{bol} is overestimated, typically by $\sim 10\text{--}15\%$. Thus, in all cases, our calculations of L_{bol} are based on the integrated fluxes of the best-fit blackbodies plotted in Fig. 1.

The resulting estimates of L_{bol} , as obtained from the blackbody fits and the distances listed in column 2 of Table 3, are listed in Table 3, column 3. The Table also lists L_{bol} values for the same stars as gleaned from the literature and (for consistency) corrected for the Gaia EDR3-based distances listed in the Table. All but two of our luminosity estimates are within $\sim 30\%$ of the literature values. The two exceptions are DR Ser, for which the Bayestar19 map yields an estimate of ISM extinction that is a factor ~ 2 larger than previously assumed (Schöier et al. 2005), and AQ And, for which the literature estimate was based on a period-luminosity relationship rather than integrated flux (Kerschbaum et al. 2010). Henceforth, we adopt the L_{bol} values obtained from our blackbody fits to dereddened photometry (i.e., the values listed in the third column of Table 3).

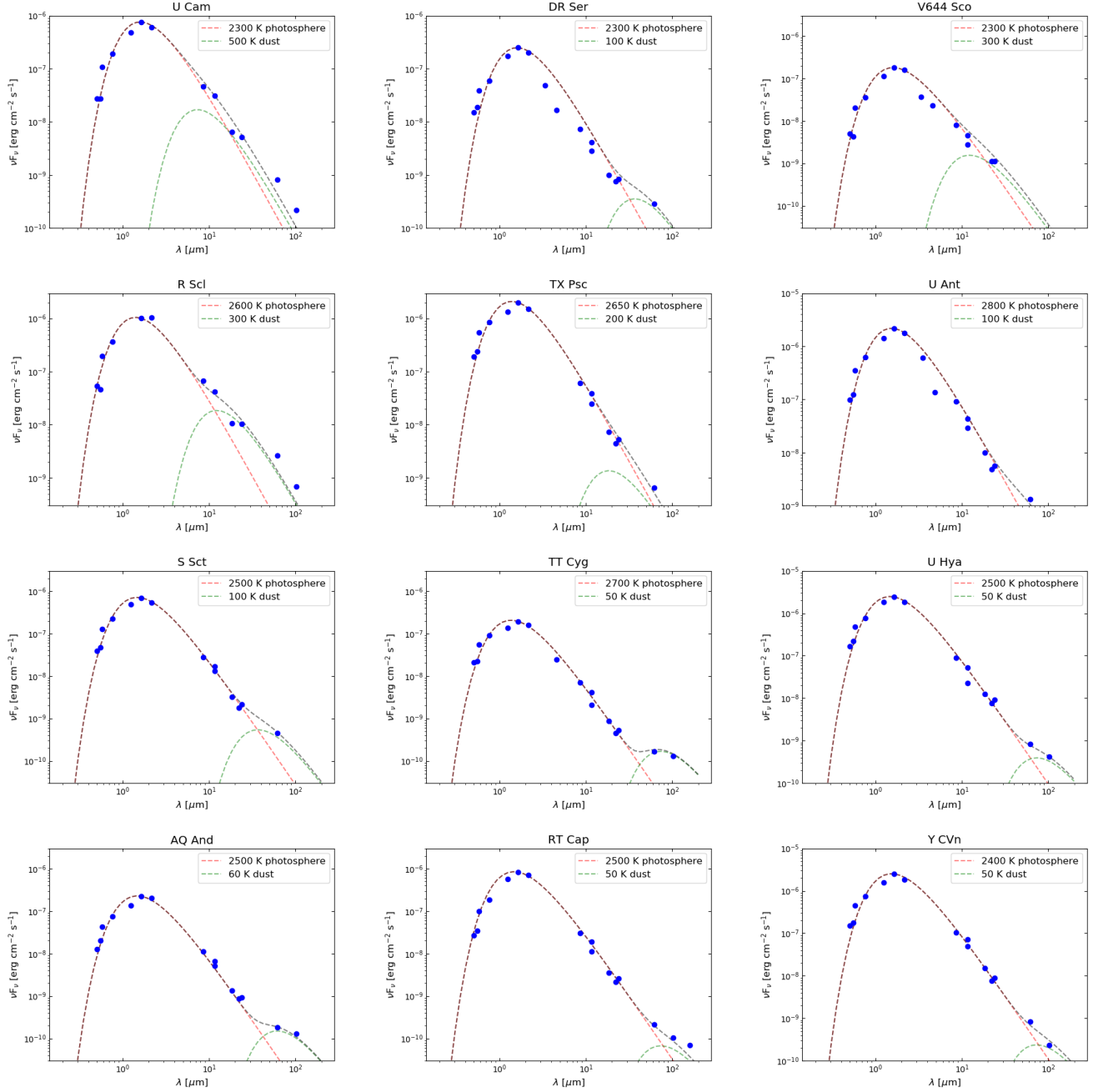


Figure 1. Optical through IR photometry for carbon stars with detached shells. Data are derived from the Gaia, 2MASS, WISE, AKARI, and/or IRAS archives (Table 2). The Gaia and 2MASS photometric data have been dereddened as described in the text. A pair of blackbodies approximating the contributions of stellar photosphere (red dashed curve) and cooler circumstellar dust (green dashed curve) is overlaid on each star’s photometry; the black dashed curve represents the composite model.

Table 3 also lists the dynamical age of the detached shell associated with each C star, τ_s . These values are obtained from the shell’s angular radius (θ_s) as reported in CO mapping observations

and/or thermal infrared emission from dust; the adopted distance, which yields the shell linear radius R_s ; and the shell expansion speed (v_s) as measured in mm-wave (rotational) lines of CO. The values of θ_s and v_s adopted for these calculations (and the references for these parameters), along with the estimates for R_s , are also compiled in Table 3. For the handful of cases where CO emission has yet to be detected from the shells themselves — three of which have the largest linear radii — we have either adopted the expansion velocity measured for the present-day CO mass loss envelope or (in one case) assumed an expansion speed of 10 km s^{-1} (see Table 1). The dynamical ages for these shells in particular — and for the larger and (hence) more evolved shells more generally — may be somewhat overestimated, if the shells had higher initial v_s (i.e., similar to the speeds of the smaller detached shells) and then were significantly decelerated as they encountered and swept up mass previously ejected by the central AGB stars (Steffen et al. 1998; Mattsson et al. 2007; Libert et al. 2007; Matthews et al. 2013). A deeper spectroscopic search for molecular or atomic gas in these very extended shells is clearly warranted, so as to establish the shell expansion speeds (indeed, deep H I observations indicate the present-day expansion speed of the Y CVn detached shell is only $\sim 1\text{--}2 \text{ km s}^{-1}$; Libert et al. 2007). It is possible that any CO in these old and very extended shells has been dissociated by interstellar UV, such that a search for 492 GHz C I line emission might be more fruitful (see Olofsson et al. 2015), although this line may not be efficiently excited at the expected low temperatures and densities that should characterize these shells.

A plot of L_{bol} vs. τ_s , obtained from the parameter values in Table 3, is presented in Fig. 2. To estimate the uncertainties on the two quantities, we have (somewhat pessimistically) assumed that the (relative) parallax errors, which are typically $\sim 15\text{--}20\%$, dominate the error propagation. This results in uncertainties in L_{bol} ranging from $\sim 20\%$ to $\sim 40\%$. If we were to instead adopt the Bailer-Jones et al. (2021) distance uncertainties (which are typically a few percent; Table 3), the ($\sim 10\text{--}30\%$) uncertainties that enter into the calculation of F_{bol} (see above) would then become the important or perhaps dominant source of error in L_{bol} , while the uncertainties in τ_s would simply shrink in direct proportion to the uncertainties in D . We further note that (as was just implied) the L_{bol} and τ_s uncertainties are correlated, since both quantities are dependent on the adopted distance. The star Y CVn well illustrates this effect: in Fig. 2, we have plotted its (L_{bol}, τ_s) positions as obtained from its Bailer-Jones et al. (2021) distance and as obtained from the inverse of its Hipparcos parallax. The discrepancy in distance translates to a significant diagonal translation of the star in L_{bol} vs. τ_s space. However, as Y CVn is the only star for which the Bailer-Jones et al. (2021) and inverse (Hipparcos) parallax distances are discrepant, it represents an extreme (indeed, unique) case in this regard.

Notwithstanding the foregoing caveats, Fig. 2 appears to reveal a U-shaped dependence of C star luminosity on detached shell age: the three C stars with the youngest detached shells (U Cam, DR Ser, V644 Sco) have the largest luminosities ($\sim 10^4 L_{\odot}$); the next three stars in detached shell age order (R Scl, TX Psc, U Ant) have somewhat ($\sim 40\%$) smaller luminosities; the next three stars (TT Cyg, S Sct, U Hya), which have “intermediate-age” shells (dynamical ages $8000\text{--}12000 \text{ yr}$), have the smallest luminosities (a few $\times 10^3 L_{\odot}$); and, finally, the three stars (AQ And, RT Cap, Y CVn) with the oldest shells (ages $\sim 20000\text{--}35000 \text{ yr}$) appear to “rebound” to luminosities in the range $\sim 5000\text{--}10000 L_{\odot}$. Fig. 2 thus suggests that detached shell C stars may be undergoing significant luminosity evolution on shell ejection timescales. Furthermore, the collective L_{bol} vs. τ_s behavior apparent in Fig. 2 — an initial steep decline in L_{bol} , followed by a slow recovery — is reminiscent of the time

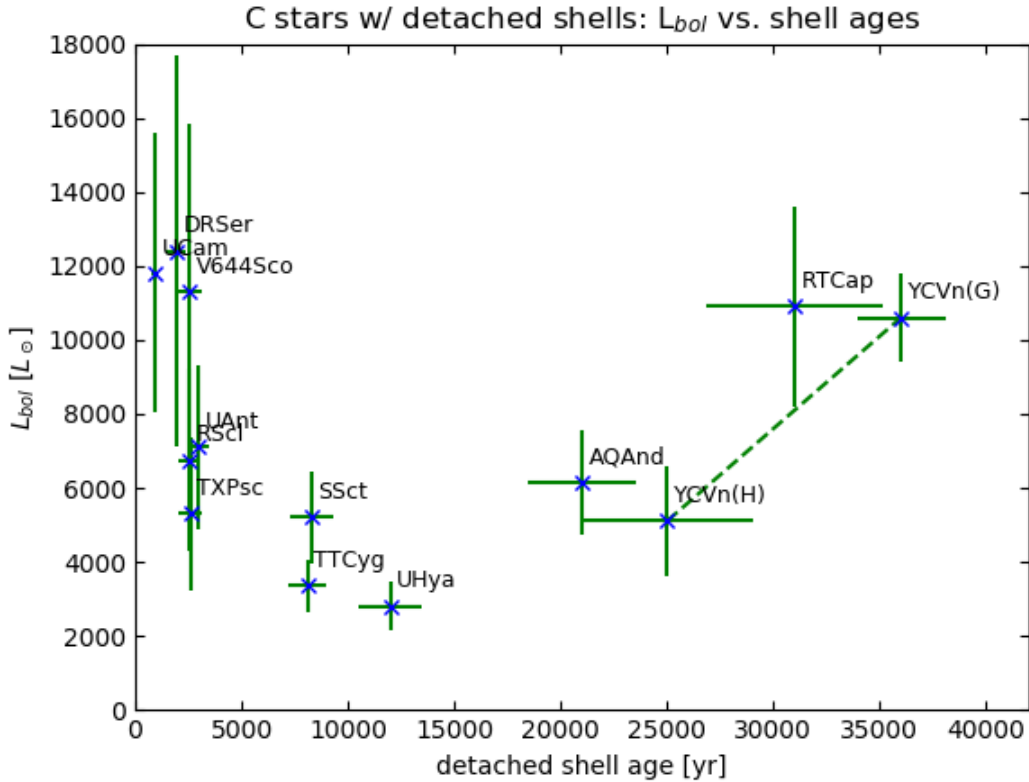


Figure 2. Bolometric luminosity (L_{bol}) vs. shell dynamical age (τ_s) for detached shell C stars (see Table 3 and § 3). The two points plotted for Y CVn represent its (L_{bol} , τ_s) positions assuming its Hipparcos (H) vs. Bailer-Jones et al. (2021) Gaia EDR3 (G) distances.

evolution of an individual AGB thermal pulse, as predicted by theory (see, e.g., Fig. 1 in Mattsson et al. 2007).

4. COMPARISON WITH MODELS

To further investigate the potential relationship between L_{bol} and τ_s for these stars, we generated models of the temporal luminosity behavior of thermally pulsing AGB stars. We used Modules for Experiments in Stellar Astrophysics (MESA; Paxton et al. 2011, 2018), release 10108, to simulate the temporal luminosity evolution of stars with initial masses 2.0, 2.8, and 3.4 M_{\odot} from the zero-age main sequence through AGB stages. The models considered here hence span a range of initial masses appropriate for C star generation on the AGB, and span the stars’ complete post-main sequence evolution at time resolutions sufficient to trace individual TPs. In the resulting MESA models, the AGB phase is but a few percent of the MS lifetime, consistent with previous detailed modeling (e.g., Herwig 2005).

The late AGB portions of the 2.0, 2.8, and 3.4 M_{\odot} models are illustrated in Fig. 3. As our focus is on AGB luminosity evolution, we did not attempt to include dredge-up and (hence) the evolution of surface C/O abundance ratio in the modeling; we note that previous approaches to modeling the relationship between TPs and C star shell ejections have assumed surface C/O >1, rather than

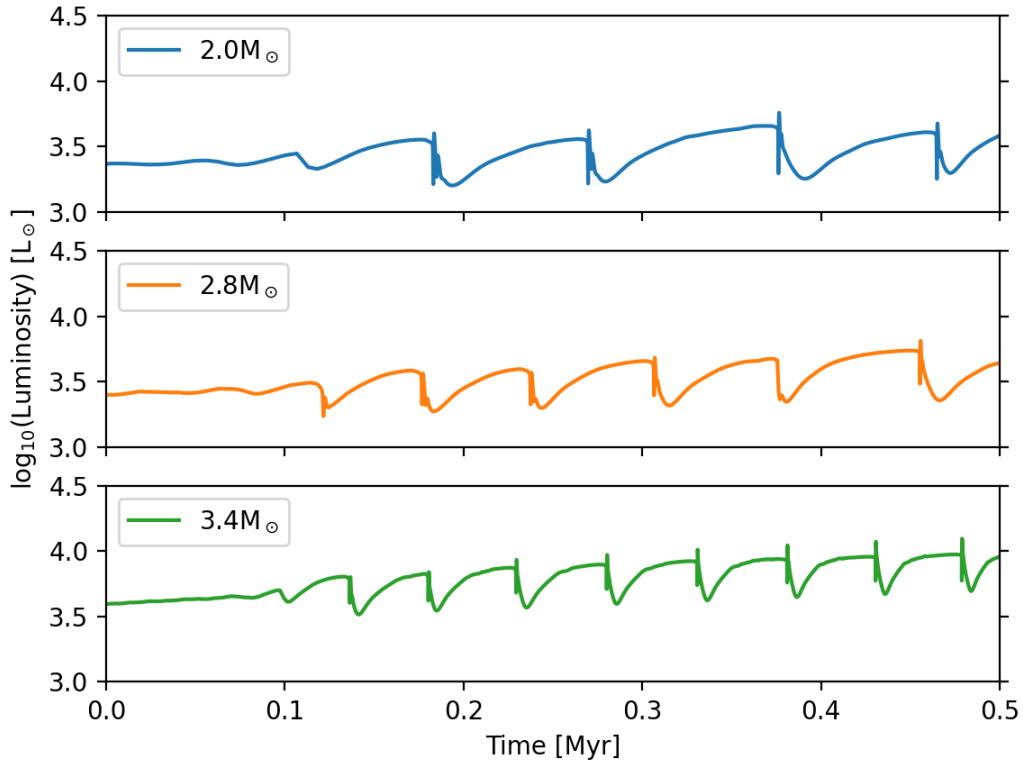


Figure 3. The late AGB portions of the 2.0, 2.8, and 3.4 M_{\odot} MESA models. The three time series shown here span 5×10^5 yr and have been aligned by applying “zero-point” time offsets of $\sim 1.2 \times 10^9$, 5.7×10^8 , and 3.1×10^8 yr, respectively, such that the onset of their TP stages roughly coincide.

attempting to model the surface C/O abundance evolution (e.g., [Mattsson et al. 2007](#)). For these simulations, we adopted the standard assumption that the AGB mass loss rate follows a “Blöcker law” (i.e., Eq. 16 in [Blöcker 1995](#)), with the mass loss rate coefficient fine-tuned to match the initial-final mass relation determined by [Cummings et al. \(2018\)](#) (see [Wilson & Nordhaus 2020](#)). However, for present purposes — tracing AGB luminosity evolution during thermal pulses — the details of mass loss, like surface C abundance, should be unimportant, so long as the internal structure of the star and, in particular, nuclear energy generation processes and rates are accurately modeled. Indeed, [Fig. 3](#) confirms that the emergent L_{bol} predicted by these AGB star models are fully consistent with previous work (see, e.g., [Fig. 5](#) in [Blöcker 1995](#)).

[Fig. 3](#) also illustrates several fundamental aspects of theoretically predicted TP AGB behavior. For example, as progenitor mass increases, the overall rise to peak AGB luminosity is steeper (faster), and this peak luminosity increases. Perhaps more importantly, for present purposes, it is immediately apparent from [Fig. 3](#) that once thermal pulsing begins, the characteristic frequency of the TP “cycles” is higher (i.e., the TP duration is shorter) for increasing progenitor mass. Also notable is the evolution in the shape of an individual TP luminosity profile for each model: the onset of a TP takes on an increasingly impulsive profile, with sharper (shorter) peaks in luminosity, as the TP portion of AGB evolution proceeds. This behavior reflects the fact that the convective transport timescale in fully

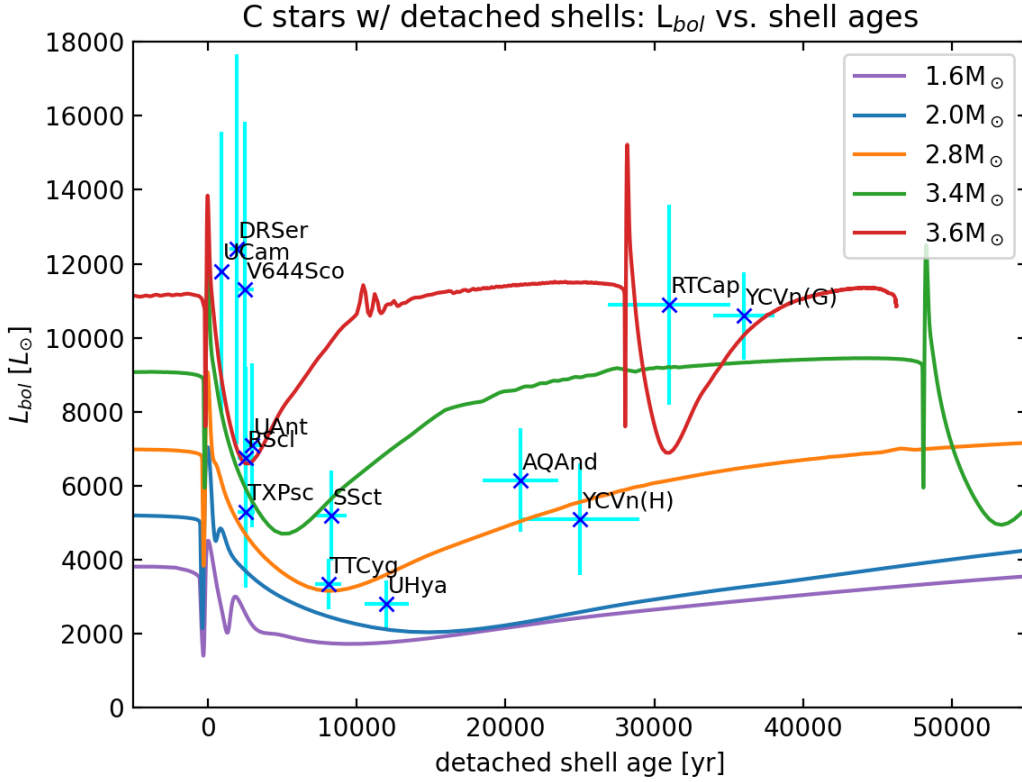


Figure 4. Detached shell C star luminosities vs. shell dynamical ages, as in Fig. 2, here compared with MESA models of the temporal evolution of individual TPs on the upper AGB for progenitor masses of 1.6, 2.0, 2.8, 3.4, and 3.6 M_{\odot} . The model L_{bol} time series are displayed such that the onset of the TPs are aligned at $\tau = 0$. The two points plotted for Y CVn again represent its positions in (L, τ) space assuming Hipparcos (H) vs. Gaia (G) distances.

convective AGB envelopes is likely on the order of years (Wilson & Nordhaus 2019), such that the energy release from a TP (He shell flash) is essentially instantaneous.

In Fig. 4, we again plot L_{bol} vs. τ_s for each detached shell C star (as in Fig. 2), but here overlaid with the luminosity vs. time profiles of individual thermal pulses, as extracted from the 2.0, 2.8, and 3.4 M_{\odot} MESA models just described. We also overlay TPs extracted from 1.6 and 3.6 M_{\odot} MESA models. The L_{bol} time series shown for each model in Fig. 4 is the most luminous TP that is modeled in its entirety; in the case of the 2.0, 2.8 and 3.4 M_{\odot} models, these are the penultimate TPs displayed in Fig. 3. The model L_{bol} time series are displayed such that the onset of these TPs are aligned at $\tau = 0$. It is readily apparent from this Figure that the collective luminosity evolution of detached shell C stars as a function of shell dynamical age is quite consistent with the theoretically predicted temporal profiles (i.e., “light curves”) of individual thermal pulses for the 2.8 M_{\odot} , 3.4 M_{\odot} , and (in the case of the highest-luminosity stars) 3.6 M_{\odot} models. Indeed, the models appear to well reproduce specific details of the collective luminosity behavior of detached shell C stars: in particular, an initial peak L approaching or exceeding $\sim 10^4 L_{\odot}$, followed by a rapid (few thousand

year) decline to luminosities of a few $\times 1000 L_{\odot}$ and, subsequently, a slow (few $\times 10^4$ yr) recovery to pre-TP luminosity levels.

Furthermore, the comparison between predicted and observed L_{bol} vs. τ_s behavior illustrated in Fig. 4 appears to constrain the range of progenitor masses that characterize detached shell C stars. Specifically, the least luminous known detached shell C stars, TT Cyg and U Hya, lie (respectively) along and just below the $2.8 M_{\odot}$ curve; whereas the most luminous stars — U Cam, DR Ser, V644 Sco, RT Cap, and (adopting its Gaia distance) Y CVn — lie along or just above the $3.6 M_{\odot}$ curve (though the TP duration for this model appears too short to be consistent with the large shell dynamical age of Y CVn, if one adopts its Gaia distance³). Hence, Fig. 4 indicates that the dozen known examples of detached shell C stars are most likely descended from $\sim 2.5\text{--}4.0 M_{\odot}$ progenitors.

In this same regard, it is intriguing that the stars S Sct, RT Cap, and U Ant display secondary dust shells with radii that range from roughly twice (S Sct, RT Cap) to ~ 6 times larger (U Ant) than those of their brighter, inner detached shells (Mećina et al. 2014; Izumiura et al. 1997). It is tempting to conclude that these faint, outlying dust shells were ejected by earlier TPs. If so, this might constrain the interpulse timescales of these stars and, hence, their progenitor masses. We note that the TP light curve for an AGB model with progenitor mass of $3.6 M_{\odot}$ has a pre-TP luminosity of $\sim 11000 L_{\odot}$ and a TP “period” of $\sim 2.8 \times 10^4$ yr. These parameters closely correspond to the approximate luminosity of RT Cap and the approximate characteristic timescale of its shell ejection sequence (assuming $v_s \approx 8 \text{ km s}^{-1}$). Similarly, the ratio of concentric dust shell radii inferred for U Ant (~ 6 ; Izumiura et al. 1997) is consistent with its position along the $3.6 M_{\odot}$ model TP light curve in Figure 4; this progenitor mass lies within the range inferred by Izumiura et al. (1997) from similar (model TP interval) considerations. On the other hand, the present-day luminosity of S Sct appears to fall far below what the models would predict if its interpulse timescale is as short as is implied by its nested shells (i.e., ~ 8000 yr, assuming the outer shell has an expansion speed similar to that of the inner shell).

5. CONCLUSIONS

We have exploited newly available Gaia parallaxes and photometry, along with archival infrared photometry, to obtain refined estimates of the luminosities of all (12) known detached shell carbon stars. We used the results to examine the relationship between these luminosities and the estimated dynamical ages (ejection times) of the detached shells associated with the 12 stars, which range from ~ 1000 to ~ 30000 yr.

We find that C stars with the youngest detached shells (dynamical ages < 3000 yr) have larger luminosities, on average, than those with intermediate-age detached shells (dynamical ages $\sim 8000\text{--}12000$ yr); many of the former exceed $\sim 10^4 L_{\odot}$, whereas the latter all have luminosities of a few $\times 10^3 L_{\odot}$. This apparent overall decline in carbon star luminosity over a $\sim 10^4$ yr timescale following shell ejection supports the hypothesis that the shell ejections are triggered by the sharp luminosity increases, and subsequent declines, that are predicted to define AGB thermal pulses (Olofsson et al. 1993; Steffen et al. 1998; Mattsson et al. 2007). Furthermore, the luminosities of the C stars with the oldest shells (dynamical ages $\sim 20000\text{--}30000$ yr) are similar to those of the C stars with young shells, suggesting these stars are in the process of a slow recovery to their pre-TP luminosities.

³ The discrepancy becomes worse if one accounts for the likelihood that the detached shell of Y CVn has undergone significant interactions with the ambient ISM (Libert et al. 2007; Matthews et al. 2013).

Overall, this collective temporal behavior appears to closely follow the predicted temporal profiles (i.e., “light curves”) of individual thermal pulses, as obtained from models of AGB stars that are descended from 2.0, 2.8, and 3.4 M_{\odot} progenitors (Fig. 4). We conclude that detached shell C stars effectively trace the luminosity evolution of AGB thermal pulses. Moreover, based on the correspondence between the observed distribution of detached shell C star luminosities vs. shell ages and the model TP temporal profiles, the progenitor masses of the majority of C stars known to exhibit detached shells appear to be restricted to the range $\sim 2.5\text{--}4.0 M_{\odot}$. The same comparison suggests that first three stars in the sequence in Fig. 4 (U Cam, DR Ser, and V644 Sco) may be descended from somewhat higher-mass progenitors. Thus, most detached shell C stars may be descended from a narrower range of progenitor masses than that estimated for Galactic C stars generally (i.e., $\sim 1.6\text{--}4.5 M_{\odot}$; Karakas 2014; Marigo et al. 2020).

Given their potential great utility as probes of AGB star luminosity, mass loss, and chemical evolution, it is noteworthy that detached shell C stars also constitute an especially elite class of AGB star. Specifically, there are ~ 120 bright C stars within ~ 1 kpc of the Sun, ~ 70 of which have detectable circumstellar CO emission indicative of mass loss rates $\gtrsim 10^{-7} M_{\odot} \text{ yr}^{-1}$ (Olofsson et al. 1993; Schöier & Olofsson 2001). Hence, the known C stars with detached shells comprise $\lesssim 15\%$ of the mass-losing C star population in the solar neighborhood. It is likely not coincidental that this fraction is similar to the fraction of time an intermediate-mass star spends on the TP (as opposed to “early”) portion of the AGB, according to theory (Blöcker 1995). The combination of the short duration of the TP AGB stage, the narrow progenitor mass range leading to AGB stars with the requisite TP behavior to eject a detached shell, and the efficient coupling between radiation pressure and wind momentum that characterizes C-rich dust might also help explain why there have thus far been relatively few unambiguous detections of detached shells associated with O-rich AGB stars (R Hya, RX Lep, and Y Uma; Hashimoto et al. 1998; Matthews et al. 2013), despite the fact that O-rich AGB stars far outnumber C stars in the Galaxy (Höfner & Olofsson 2018).

Indeed, given that engulfment of a close binary companion could truncate AGB evolution well before the TP stage commences (e.g., Wilson & Nordhaus 2019), it is actually surprising that detached shell C stars are not an even rarer breed. However, of the dozen known examples, only R Scl displays clear evidence for the impact of binarity on its mass loss history, in the form of spiral structure imprinted on its detached shell (Maercker et al. 2016). Thus, most C stars with detached shells appear to offer examples of “pure” single-star evolution to the tip of the AGB, for stars of initial mass $\sim 2.5\text{--}3.5 M_{\odot}$. This further implies that the relatively rare (distant) examples of unusually luminous, highly dust-enshrouded Galactic C stars that exhibit large ($\sim 15\text{--}30 \text{ km s}^{-1}$) CO outflow velocities (Kastner et al. 1993) may be AGB stars descended from $\sim 2.5\text{--}4.5 M_{\odot}$ progenitors that we happen to be observing at or just after (within ~ 1000 yr of) the luminosity peaks of their thermal pulse cycles.

ACKNOWLEDGMENTS

J.H.K. wishes to thank Franz Kerschbaum, Sofia Ramstedt, and Matthias Maercker, the lead organizers of “A Star Has Evolved: a Conference in the Honour of Hans Olofsson” (held August 2019 in Smögen, Sweden), as well as Hans Olofsson himself, for providing the inspiration for this paper. The authors also thank the anonymous referee, as well as Rens Waters, Hideyuki Izumiura, and Thibaut Le Bertre, for helpful comments that improved the manuscript. E.W.’s research is supported by National Science Foundation grant NSF-2009713 to RIT.

REFERENCES

- Bailer-Jones, C. A. L. 2015, *PASP*, 127, 994, doi: [10.1086/683116](https://doi.org/10.1086/683116)
- Bailer-Jones, C. A. L., Rybizki, J., Fouesneau, M., Demleitner, M., & Andrae, R. 2021, *AJ*, 161, 147, doi: [10.3847/1538-3881/abd806](https://doi.org/10.3847/1538-3881/abd806)
- Bergeat, J., Knapik, A., & Rutily, B. 2001, *A&A*, 369, 178, doi: [10.1051/0004-6361:20010106](https://doi.org/10.1051/0004-6361:20010106)
- Blöcker, T. 1995, *A&A*, 297, 727
- Brunner, M., Mecina, M., Maercker, M., et al. 2019, *A&A*, 621, A50, doi: [10.1051/0004-6361/201833652](https://doi.org/10.1051/0004-6361/201833652)
- Cummings, J. D., Kalirai, J. S., Tremblay, P. E., Ramirez-Ruiz, E., & Choi, J. 2018, *ApJ*, 866, 21, doi: [10.3847/1538-4357/aadfd6](https://doi.org/10.3847/1538-4357/aadfd6)
- Gaia Collaboration, Brown, A. G. A., Vallenari, A., et al. 2021, *A&A*, 649, A1.
- Green, G. M., Schlafly, E., Zucker, C., Speagle, J. S., & Finkbeiner, D. 2019, *ApJ*, 887, 93, doi: [10.3847/1538-4357/ab5362](https://doi.org/10.3847/1538-4357/ab5362)
- Hashimoto, O., Izumiura, H., Kester, D. J. M., & Bontekoe, T. R. 1998, *A&A*, 329, 213
- Herwig, F. 2005, *ARA&A*, 43, 435, doi: [10.1146/annurev.astro.43.072103.150600](https://doi.org/10.1146/annurev.astro.43.072103.150600)
- Höfner, S., & Olofsson, H. 2018, *A&A Rv*, 26, 1, doi: [10.1007/s00159-017-0106-5](https://doi.org/10.1007/s00159-017-0106-5)
- Izumiura, H., Hashimoto, O., Kawara, K., Yamamura, I., & Waters, L. B. F. M. 1996, *A&A*, 315, L221
- Izumiura, H., Ueta, T., Yamamura, I., et al. 2011, *A&A*, 528, A29, doi: [10.1051/0004-6361/201015163](https://doi.org/10.1051/0004-6361/201015163)
- Izumiura, H., Waters, L. B. F. M., de Jong, T., et al. 1997, *A&A*, 323, 449
- Karakas, A. I. 2014, *MNRAS*, 445, 347, doi: [10.1093/mnras/stu1727](https://doi.org/10.1093/mnras/stu1727)
- Kastner, J. H., Forveille, T., Zuckerman, B., & Omont, A. 1993, *A&A*, 275, 163
- Kerschbaum, F., Ladjal, D., Ottensamer, R., et al. 2010, *A&A*, 518, L140, doi: [10.1051/0004-6361/201014633](https://doi.org/10.1051/0004-6361/201014633)
- Kerschbaum, F., Maercker, M., Brunner, M., et al. 2017, *A&A*, 605, A116, doi: [10.1051/0004-6361/201730665](https://doi.org/10.1051/0004-6361/201730665)
- Lallement, R., Babusiaux, C., Vergely, J. L., et al. 2019, *A&A*, 625, A135, doi: [10.1051/0004-6361/201834695](https://doi.org/10.1051/0004-6361/201834695)
- Libert, Y., Gérard, E., & Le Bertre, T. 2007, *MNRAS*, 380, 1161, doi: [10.1111/j.1365-2966.2007.12154.x](https://doi.org/10.1111/j.1365-2966.2007.12154.x)
- Lindegren, L., Klioner, S. A., Hernández, J., et al. 2021, *A&A*, 649, A2, doi: [10.1051/0004-6361/202039709](https://doi.org/10.1051/0004-6361/202039709)
- Lindqvist, M., Olofsson, H., Lucas, R., et al. 1999, *A&A*, 351, L1
- Maercker, M., Khouri, T., De Beck, E., et al. 2018, *A&A*, 620, A106, doi: [10.1051/0004-6361/201833665](https://doi.org/10.1051/0004-6361/201833665)
- Maercker, M., Mohamed, S., Vlemmings, W. H. T., et al. 2012, *Nature*, 490, 232, doi: [10.1038/nature11511](https://doi.org/10.1038/nature11511)
- Maercker, M., Vlemmings, W. H. T., Brunner, M., et al. 2016, *A&A*, 586, A5, doi: [10.1051/0004-6361/201527128](https://doi.org/10.1051/0004-6361/201527128)
- Marigo, P., Girardi, L., Bressan, A., et al. 2008, *A&A*, 482, 883, doi: [10.1051/0004-6361:20078467](https://doi.org/10.1051/0004-6361:20078467)
- Marigo, P., Cummings, J. D., Curtis, J. L., et al. 2020, *Nature Astronomy*, 4, 1102, doi: [10.1038/s41550-020-1132-1](https://doi.org/10.1038/s41550-020-1132-1)
- Matthews, L. D., Le Bertre, T., Gérard, E., et al. 2013, *AJ*, 145, 97, doi: [10.1088/0004-6256/145/4/97](https://doi.org/10.1088/0004-6256/145/4/97)
- Mattsson, L., Höfner, S., & Herwig, F. 2007, *A&A*, 470, 339, doi: [10.1051/0004-6361:20066368](https://doi.org/10.1051/0004-6361:20066368)
- Mecina, M., Kerschbaum, F., Groenewegen, M. A. T., et al. 2014, *A&A*, 566, A69, doi: [10.1051/0004-6361/201321117](https://doi.org/10.1051/0004-6361/201321117)
- Olofsson, H., Bergman, P., Eriksson, K., & Gustafsson, B. 1996, *A&A*, 311, 587
- Olofsson, H., Bergman, P., & Lindqvist, M. 2015, *A&A*, 582, A102, doi: [10.1051/0004-6361/201526741](https://doi.org/10.1051/0004-6361/201526741)
- Olofsson, H., Carlstrom, U., Eriksson, K., & Gustafsson, B. 1992, *A&A*, 253, L17
- Olofsson, H., Carlstrom, U., Eriksson, K., Gustafsson, B., & Willson, L. A. 1990, *A&A*, 230, L13
- Olofsson, H., Eriksson, K., & Gustafsson, B. 1988, *A&A*, 196, L1
- Olofsson, H., Eriksson, K., Gustafsson, B., & Carlstrom, U. 1993, *ApJS*, 87, 267, doi: [10.1086/191804](https://doi.org/10.1086/191804)
- Paxton, B., Bildsten, L., Dotter, A., et al. 2011, *ApJS*, 192, 3, doi: [10.1088/0067-0049/192/1/3](https://doi.org/10.1088/0067-0049/192/1/3)

- Paxton, B., Schwab, J., Bauer, E. B., et al. 2018, *ApJS*, 234, 34, doi: [10.3847/1538-4365/aaa5a8](https://doi.org/10.3847/1538-4365/aaa5a8)
- Ramstedt, S., Maercker, M., Olofsson, G., Olofsson, H., & Schöier, F. L. 2011, *A&A*, 531, A148, doi: [10.1051/0004-6361/201015964](https://doi.org/10.1051/0004-6361/201015964)
- Ramstedt, S., Vlemmings, W. H. T., Doan, L., et al. 2020, *A&A*, 640, A133, doi: [10.1051/0004-6361/201936874](https://doi.org/10.1051/0004-6361/201936874)
- Schlafly, E. F., & Finkbeiner, D. P. 2011, *ApJ*, 737, 103, doi: [10.1088/0004-637X/737/2/103](https://doi.org/10.1088/0004-637X/737/2/103)
- Schöier, F. L., Lindqvist, M., & Olofsson, H. 2005, *A&A*, 436, 633, doi: [10.1051/0004-6361:20042510](https://doi.org/10.1051/0004-6361:20042510)
- Schöier, F. L., & Olofsson, H. 2001, *A&A*, 368, 969, doi: [10.1051/0004-6361:20010072](https://doi.org/10.1051/0004-6361:20010072)
- Steffen, M., Szczerba, R., & Schoenberner, D. 1998, *A&A*, 337, 149
- Van Langevelde, H., Quiroga-Nuñez, L. H., Vlemmings, W. H. T., et al. 2018, in 14th European VLBI Network Symposium & Users Meeting (EVN 2018), 43. <https://arxiv.org/abs/1901.07804>
- van Leeuwen, F. 2007, *A&A*, 474, 653, doi: [10.1051/0004-6361:20078357](https://doi.org/10.1051/0004-6361:20078357)
- Vlemmings, W. H. T., Khouri, T., & Olofsson, H. 2019, *A&A*, 626, A81, doi: [10.1051/0004-6361/201935329](https://doi.org/10.1051/0004-6361/201935329)
- Wilson, E. C., & Nordhaus, J. 2019, *MNRAS*, 485, 4492, doi: [10.1093/mnras/stz601](https://doi.org/10.1093/mnras/stz601)
- . 2020, *MNRAS*, 497, 1895, doi: [10.1093/mnras/staa2088](https://doi.org/10.1093/mnras/staa2088)